Biochimica et Biophysica Acta 1838 (2014) 106–116

Contents lists available at ScienceDirect

Biochimica et Biophysica Acta

journal homepage: www.elsevier.com/locate/bbamem

Conformational changes of the bacterial type I ATP-binding cassette importer $HisQMP_2$ at distinct steps of the catalytic cycle

Johanna Heuveling [a], Violette Frochaux [b], Joanna Ziomkowska [c], Robert Wawrzinek [d], Pablo Wessig [d], Andreas Herrmann [c], Erwin Schneider [a,*]

[a] Institut für Biologie/Bakterienphysiologie, Humboldt Universität zu Berlin, Chausseestr. 117, D-10115 Berlin, Germany
[b] Institut für Chemie, Humboldt Universität zu Berlin, Brook-Taylor-Str. 2, D-12489 Berlin, Germany
[c] Institut für Biologie/Molekulare Biophysik, Humboldt Universität zu Berlin, Invalidenstr. 42, D-10115 Berlin, Germany
[d] Institut für Chemie, Universität Potsdam, Karl-Liebknecht-Str. 24-25, D-14476 Potsdam, Germany

ARTICLE INFO

Article history:
Received 23 July 2013
Received in revised form 27 August 2013
Accepted 30 August 2013
Available online 7 September 2013

Keywords:
ABC transporter
Type I importer
Histidine transport
Limited proteolysis
Fluorescence lifetime
Alternate access model

ABSTRACT

Prokaryotic solute binding protein-dependent ATP-binding cassette import systems are divided into type I and type II and mechanistic differences in the transport process going along with this classification are under intensive investigation. Little is known about the conformational dynamics during the catalytic cycle especially concerning the transmembrane domains. The type I transporter for positively charged amino acids from *Salmonella enterica* serovar Typhimurium ($LAO\text{-}HisQMP_2$) was studied by limited proteolysis in detergent solution in the absence and presence of co-factors including ATP, ADP, LAO/arginine, and Mg^{2+} ions. Stable peptide fragments could be obtained and differentially susceptible cleavage sites were determined by mass spectrometry as Lys-258 in the nucleotide-binding subunit, HisP, and Arg-217/Arg-218 in the transmembrane subunit, HisQ. In contrast, transmembrane subunit HisM was gradually degraded but no stable fragment could be detected. HisP and HisQ were equally resistant under pre- and post-hydrolysis conditions in the presence of arginine-loaded solute-binding protein LAO and ATP/ADP. Some protection was also observed with LAO/arginine alone, thus reflecting binding to the transporter in the apo-state and transmembrane signaling. Comparable digestion patterns were obtained with the transporter reconstituted into proteoliposomes and nanodiscs. Fluorescence lifetime spectroscopy confirmed the change of HisQ(R218) to a more apolar microenvironment upon ATP binding and hydrolysis. Limited proteolysis was subsequently used as a tool to study the consequences of mutations on the transport cycle. Together, our data suggest similar conformational changes during the transport cycle as described for the maltose ABC transporter of *Escherichia coli*, despite distinct structural differences between both systems.

1. Introduction

ATP-binding cassette (ABC) transporters are membrane proteins that mediate the uptake or export of an enormous variety of substrates at the expense of ATP. They are found in all organisms from bacteria to man and dysfunction is often associated with disease [1]. Canonical ABC import systems of prokaryotes are built up of two transmembrane domains (TMD) forming a translocation path, a dimeric nucleotide binding domain (NBD) that energizes the transport by hydrolysis of ATP, and an extracellular high affinity substrate-binding protein (SBP) [2,3]. By their structure and size and due to biochemical analysis prokaryotic ABC importers can be classified as type I and type II import systems [4].

As mechanism of transport, the "alternate access" model was proposed based on biophysical and structural data [5–7]. Triggered by signals like SBP-binding, ATP-binding, ATP-hydrolysis, and ADP-release which are transmitted over the TMDs by largely unknown mechanisms, alternating inward- and outward-facing conformations are assumed causing shuttling of the substrate to the cytoplasm (reviewed in Ref. [8]). Although generally accepted, mechanistical variations are likely to exist between type I and type II transporters. While the vitamin B_{12} importer $Btu(CD)_2$, a type II importer, binds its cognate receptor, BtuF, with high affinity in its substrate-free form and in the absence of nucleotides, it loses affinity upon ATP- or substrate binding [9]. The maltose transporter, $MalFGK_2$, as a representative of type I importers, on the other hand seems to be associated with its solute binding protein, MalE, throughout the transport cycle, however with much lower affinity [10–12]. The movements of the TMD as well seem to result from opposing signals when comparing both systems [7,13,14]. These findings as

Abbreviations: ABC, ATP-binding cassette; DBD, [1,3]dioxolo[4,5-f][1,3]benzodioxole; DDM, n-dodecyl-β-D-maltopyranoside; His-tag, hexahistidine tag; IPTG, isopropyl-β-D-thio-galactopyranoside; MSP, membrane scaffold protein; MOPS, (3-(N-morpholino)-propanesulfonic acid); NBD, nucleotide binding domain; OG, octyl-β-D-glucopyranoside; PMSF, phenylmethylsulfonylfluoride; SBP, solute binding protein; TMD, transmembrane domain

* Corresponding author. Tel.: +49 30 20938121; fax: +49 30 20938126.
E-mail address: erwin.schneider@rz.hu-berlin.de (E. Schneider).

0005-2736/$ – see front matter © 2013 Elsevier B.V. All rights reserved.
http://dx.doi.org/10.1016/j.bbamem.2013.08.024

well as those from a comparative investigation of two molybdate transporters of type I and type II, respectively [15], suggest that variations of the mechanism and more experimental evidence from other systems are required to clarify whether they go along with the classification of importers as type I and II. A first exception from this notion was postulated by Doeven et al. [16], who demonstrated by fluorescence correlation spectroscopy that the binding protein of the oligopeptide ABC transporter of *Lactococcus lactis*, a type I importer, moved away from the membrane components upon binding of ATP to the ATPase subunits. Furthermore, due to some unique features of the maltose transporter [6], it is also questionable whether the derived transport model holds for other type I ABC importers.

The type I histidine ABC transporter of *Salmonella enterica* serovar Typhimurium (*S.* Typhimurium) is well characterized by biochemical and biophysical means [17–20]. It consists of the transmembrane subunits HisQ and HisM, each spanning the lipid bilayer five times [21], and a homodimer of the nucleotide-binding subunit, HisP. Substrates are delivered by two solute binding proteins, HisJ with preference for histidine, and LAO with highest affinities for lysine, arginine and ornithine. While crystal structures of HisJ [22], LAO [23], and HisP [24] are available, structural information on the complete transporter is elusive. HisJ/LAO binds to $HisQMP_2$ in unliganded and substrate-loaded form with relatively low affinity [25]. The opening and closing of the $HisP_2$ dimer have been studied by fluorescence spectroscopy and sulfhydryl modification [26] as well as by molecular dynamics simulations [27], but little is known on conformational changes of the TMDs during the transport cycle.

In this communication, limited proteolysis was used as a tool to monitor conformational changes of the TMDs and NBDs of the histidine transporter. This approach, supported by fluorescence lifetime data, provided further insights into the dynamics and signaling during the catalytic cycle. Moreover it was proven useful in characterizing the conformational defects of transporter variants.

2. Material and methods

2.1. Bacterial strains, plasmids, and media

Strains and plasmids used in this study are summarized in Table 1. *Escherichia coli* strain JM109 served as a host for general cloning purposes and strain BL21 (DE3) pLysS-T1^R for overproduction of proteins. Bacteria were usually grown in LB [28] or TB [29] medium, supplemented with ampicillin (100 μg/ml) and/or chloramphenicol (15 μg/ml) if required.

Table 1
Bacterial strains and plasmids used in this study.

Strain or plasmid	Relevant genotype or description	Reference or source
Escherichia coli strains		
JM109	e14$^-$ (*mcrA*) *recA1 endA1 gyrA96 thi-1 hsdR17* (r_K^- m_K^+) *supE44 relA1* Δ(*lac-proAB*) F′[*traD36 proAB*$^+$ *lacI*^{q} *lacZ*ΔM15]	Stratagene (La Jolla, CA)
BL21 (DE3) pLysS-T1^R	F− *ompT hsdS*$_B$(r_B^- m_B^-) *gal dcm* λ (DE3) *tonA* pLysS (Cm^R)	Sigma Aldrich (Germany)
Plasmids		
Expression vectors		
pET15b	Ap^r, p_{T7lac}, His_6 coding sequence (5′), thrombin cleavage site	Novagen
pET22b	Ap^r, p_{T7lac}, His_6 coding sequence (3′)	Novagen
*argT***-hisJQMP plasmids of S. Typhimurium*		
pVE26	*hisQMP* on pET22b	[30]
pSN3	*argT* on pET15b	Lab collection
pVE27	*hisQMP*(T205A) on pET22b	[46]
pJH5	*hisQMP*(E179Q) on pET22b	This study
pJH26	*hisQMP*(R248H) on pET22b	This study
pJH30	*hisQMP*(K254H) on pET22b	This study
pJH31	*hisQMP*(K258H) on pET22b	This study
pJH33	*hisQ*(R217H, R218H)*MP* on pET22b	This study
pKB2	*hisQ*(R218C)**M***P** on pET22b	This study
pJH42	*hisP* on pET22b	This study

*The *argT* gene encodes the lysine/arginine/ornithine-binding protein LAO.

2.2. Site-directed mutagenesis and cloning of hisP

Mutagenesis of *hisQMP* was carried out using QuikChange Lightning site-directed mutagenesis Kit (Stratagene, La Jolla, CA) according to the manufacturer's instructions. Oligonucleotides were purchased from Sigma Aldrich (Germany) and are listed in Table S1. Sequencing was carried out by SMB Services in Molecular Biology GmbH (Berlin, Germany).

The *hisP* wild type allele was cloned by PCR amplification using pVE26 (*hisQMP*) as template with oligonucleotides containing restriction sites for subsequent ligation into a pET22b vector. The resulting plasmid was named pJH 42 (Table 1).

2.3. Protein purification

LAO-His_6 was purified from the cytosolic fraction of *E. coli* strain BL21 (DE3) pLysS T1^R harboring plasmid pSN3 by metal-affinity chromatography on a TALON resin as described elsewhere [30,31]. The His-tag was cleaved off by treatment with thrombin (Thrombin CleanCleave™ Kit, Sigma-Aldrich, Germany) according to the manufacturer's instructions. The protein was concentrated by a centrifugal device (Amicon, Millipore, Germany) and buffered in 50 mM MOPS/K^+ (pH 7.5), 5% (v/v) glycerol, 0.15 M NaCl by passage through a PD10 desalting column (GE Healthcare).

For overproduction and purification of HisQM(P-His_6)$_2$ (wild type and variants), *E. coli* strain BL21 (DE3) pLysS T1^R was transformed with pVE26 or its derivatives and grown in TB-ampicillin/chloramphenicol to an OD_{650} of 0.8 prior to the addition of 0.1 mM IPTG. Cells were harvested after overnight growth at 22 °C and the membrane fraction was obtained by passage of cells through a French press and subsequent ultracentrifugation (1.5 h at 200,000 × *g*). Membrane proteins were solubilized by incubation with 1.1% DDM in the presence of 50 mM MOPS/K^+ (pH 7.5), 10% (v/v) glycerol, 0.1 mM PMSF for 1 h at 4 °C. After ultracentrifugation (1 h at 200,000 × *g*), HisQM(P-His_6)$_2$ was purified by metal-affinity chromatography using a TALON resin in the presence of 50 mM MOPS/K^+ (pH 7.5), 10% (v/v) glycerol, 0.1 mM PMSF, 0.05% DDM, 4 mM β-mercaptoethanol. After washing the resin with buffer in the presence of 10 mM imidazole, protein was eluted with 100 mM imidazole. Protein-containing fractions were pooled, concentrated by a centrifugal device (Amicon, Millipore, Germany) and buffered in 50 mM MOPS/K^+ (pH 7.5), 20% (v/v) glycerol, 0.1 M NaCl, 0.02% DDM by passage through a PD10 desalting column (GE Healthcare).

For purification of HisP-His_6 *E. coli* strain BL21 (DE3) pLysS T1^R harboring plasmid pJH42 was grown at 30 °C in LB-ampicillin/chloramphenicol to an OD_{650} of 0.5 prior to the addition of 0.5 mM IPTG, and harvested 3 h later. The cells were resuspended in 50 mM MOPS/K^+ (pH 7.5), 0.1 M NaCl, 0.1 mM PMSF and disintegrated by ultrasonication. HisP-His_6 was purified from the cytosolic fraction by metal-affinity chromatography on a TALON resin equilibrated in 50 mM MOPS/K^+ (pH 7.5), 0.15 M NaCl, 5% (v/v) glycerol, 0.1 mM PMSF. After binding and washing the resin with buffer supplemented with 20 mM imidazole pH 8.0, protein was eluted with buffer containing 100 mM imidazole. Protein-containing fractions were pooled, concentrated by a centrifugal device (Amicon, Millipore, Germany) and buffered in 50 mM MOPS/K^+ (pH 7.5), 0.1 M NaCl, 10% (v/v) glycerol by passage through a PD10 desalting column (GE Healthcare). Before determination of protein concentration and trypsin digestion, the preparation was ultracentrifuged at 163,000 ×*g* for 30 min to remove aggregated protein.

Protein concentration was determined using the BCA Kit of Uptima-Interchim (France).

2.4. Preparation of proteoliposomes

Proteoliposomes containing HisQM(P-His_6)$_2$ or its variants were essentially prepared as described in [30]. *E. coli* total lipids (Avanti Polar Lipids) were dried in a rotating vacuum evaporator, redissolved in 50 mM MOPS/K^+ (pH 7.5), 1% OG to 20 mg/ml lipid, and sonicated for 15 min. For subsequent ATPase activity assay, HisQM(P-His_6)$_2$ (50 μg) was mixed with 125 μl lipid solution and 50 mM MOPS/K^+ (pH 7.5) to yield a final volume of 300 μl. Proteoliposomes were formed by removal of detergent by adsorption to Biobeads (Bio-Rad, Germany) at 4 °C overnight. After replacement with fresh Biobeads incubation continued for 1 h. Proteoliposomes were recovered by ultracentrifugation for 30 min at 163,000 ×*g*, and resuspended in 50 mM MOPS/K^+ (pH 7.5). For limited proteolysis, the proteoliposomes were resuspended in one third of the volume. The concentration and insertion rate of the complex protein was determined by SDS gel electrophoresis and pixel analysis.

2.5. Preparation of nanodiscs

Nanodiscs containing HisQM(P-His_6)$_2$ or its variants were essentially prepared as described in [32] using tagless membrane scaffold protein (MSP1E3D1) and *E. coli* total lipids (Avanti Polar Lipids). 8.3 mg lipid was dried in a rotating vacuum evaporator and kept in an exsiccator under vacuum overnight. Subsequently, the dried lipid film was resuspended in 900 μl 20 mM MOPS (pH 7.5), 0.1 M NaCl, DDM (87 μl of a 10% solution) was added and the mixture was sonicated for 15 min in a bathtype sonicator. Complex protein (1.8 mg), MSP (3.24 mg) and the lipid preparation were mixed at a molar ratio of 1:8:960. Buffer was added to reduce the glycerol concentration to below 3%, and the mixture was incubated at 4 °C for 1 h. Biobeads (1.5 mg) were added and the reconstitution mixture was incubated at 4 °C for 4 h under gentle shaking. Purification of assembled nanodiscs with complex proteins was performed by metal-affinity chromatography using a TALON resin in the presence of 50 mM MOPS/K^+ (pH 7.5), 50 mM NaCl, thereby taking advantage of the His_6 tag at the C-terminal end of the HisP subunits. After washing the resin with buffer in the presence of 25 mM imidazole, protein was eluted with 250 mM imidazole. Protein-containing fractions were pooled, concentrated and buffered in 50 mM MOPS/K^+ (pH 7.5) by passage through a PD10 desalting column (GE Healthcare). The concentration was determined by pixel analysis following SDS PAGE. Since two MSP molecules form a single nanodisc, an MSP to HisP ratio of 1:1, as inferred by the pixel analysis, indicates that one $HisQMP_2$ complex was present per nanodisc (see Fig. 2B).

2.6. ATPase activity assay

ATPase activity was assayed essentially as described previously [18,30]. Detergent-solubilized or reconstituted complex was preheated for 3 min at 37 °C in the presence or absence of 0.4 mg/ml LAO and L-arginine (1 mM). Reactions were started by the addition of ATP and $MgCl_2$ to yield a final concentration of 2 and 10 mM (3 mM in case of proteoliposomes or nanodiscs), respectively. Aliquots (25 μl) containing 4 μg detergent-solubilized or 2 μg reconstituted HisQM(P-His_6)$_2$ complex were taken over a time period of 4 min and mixed with 25 μl 12% sodium dodecyl sulfate (SDS) solution. The amount of phosphate was determined colorimetrically, using Na_2HPO_4 as the standard.

2.7. Limited proteolysis

HisQM(P-His_6)$_2$ (3.6 μM) in detergent solution (50 mM MOPS/K^+, pH 7.5, 20% glycerol, 0.02% DDM, 0.1 M NaCl) or HisQM(P-His_6)$_2$ (3 μM) reconstituted in proteoliposomes or nanodiscs in 50 mM MOPS/K^+ (pH 7.5) or HisP-His_6 (7.2 μM) in 50 mM MOPS (pH 7.5), 0.1 M NaCl, 10% glycerol were incubated in the absence and presence of co-factors as indicated to reach final concentrations of 10 mM ATP, 10 mM ADP, 3 mM $MgCl_2$, and 11 μM LAO/L-arginine (1 mM). The samples were incubated for 20 min at 37 °C, followed by 10 min at 25 °C prior to the addition of trypsin (Sigma Aldrich, Germany) to a final concentration of 3 μM (long degradation assay) and 0.3 μM (short degradation assay), respectively. Samples were taken at the indicated time points, mixed with 10× SDS-PAGE sample buffer and shock frozen in liquid nitrogen. Before loading of the samples onto the SDS PAGE gel the samples were heated to 95 °C for 5 min. Quantitation of the bands was done by pixel analysis with GelScan V5.0.

2.8. Mass spectrometry-based proteomic analysis

For nanoHPLC/ESI-MS/MS, an 1100 HPLC system (Agilent) was used. Separation was performed on a Zorbax 300 SB-C18 (150 mm × 75 μm; Agilent) column with a Zorbax 300 SB-C18 (0.3 mm × 5 mm; Agilent) enrichment column and a binary mobile phase water/acetonitrile gradient with a maximum flow rate of 0.30 μl/min. Peptides were separated using a 35 min gradient. The eluents used were as follows: A, 94.9% deionized water, 5% acetonitrile, 0.1% formic acid (v/v/v); and B, 99.9% acetonitrile, 0.1% (v/v) formic acid. The separation column was coupled to a Finnigan LTQ FT ULTRA mass spectrometer (Thermo Fisher Scientific, Bremen, Germany) using a nanomate ESI interface (Advion) working at 1.7 kV. Positive ionization and a transfer capillary temperature of 200 °C were applied. Product ions were detected in the FTICR cell and collision induce dissociation (CID) was performed in the IonTrap with data-dependent fragmentation and normalized collision energy of 35%. Proteome Discoverer 1.2 (Thermo) was used to analyze the data. For the identification the database uniprot and swissprot were chosen. Identification parameters: enzyme trypsin or chymotrypsin with 2 missed cleavages, modifications: deamidated (N), oxidation (M) and propionamide (C), Tolerance: 5 ppm for the precursor mass tolerance and 0.5 Da for the fragment mass tolerance. A reverse database was used to prevent false positive identification.

2.9. In-gel digestion

For in-gel digestion selected protein spots were cut out, transferred to vials, and washed three times using 200 μl (50% acetonitrile, and 50% 25 mM ammonium hydrogen carbonate (v/v)). Then the gel pieces were dehydrated using 50 μl acetonitrile. The supernatant was removed and the gel pieces were dried for 20 min at 37 °C. 20 to 30 μl of modified trypsin (0.01 g/l, Promega) in 25 mM ammonium hydrogen carbonate or chymotrypsin (0.04 g/l, Sigma Aldrich) in 100 mM Tris–HCl (pH 8), 10 mM $CaCl_2$ was added subsequently and after 30 min 20 μl of 25 mM ammonium hydrogen carbonate buffer was added to each vial; trypsin and chymotrypsin digestion was carried out for 12 h at 37 °C. After centrifugation, the supernatant was carefully removed, and the peptides were extracted twice from the gel by adding 50 μl of the following extraction solution: 50% acetonitrile, 50% formic acid (5%). Finally all pellets were extracted with 50 μl of acetonitrile. The supernatants were pooled, evaporated to dryness by a vacuum concentrator and redissolved in 20 μl 0.1% formic acid (v/v) for analysis.

2.10. Fluorescence labeling and spectroscopy

For fluorescence lifetime spectroscopy the single cysteine variant HisQ(R218C)MP_2 was chemically labeled with a maleimide tagged fluorescent acyl [1,3] dioxolo[4,5-*f*] [1,3] benzodioxole (DBD) (compound 32) [33,34]. The purified protein in 50 mM MOPS/K^+ (pH 7.5), 20% (v/v) glycerol, 0.1 M NaCl, 0.02% DDM was incubated with a tenfold molar excess of acyl-DBD-maleimide at 4 °C, overnight. Subsequently, excess of fluorescent dye was removed by size exclusion chromatography using a PD10 column (GE Healthcare Life Sciences). The fluorescence lifetime measurements were performed on a PicoQuant PDL 200 pulsed Laser Diode Fluorescence Lifetime Spectrometer. A 470 nm excitation laser (PicoQuant) with 4 MHz repetition frequency was used. The

emission signal was detected at 593 nm (66 ps resolution). Labeled HisQ(R218C)M(P-His_6)$_2$ (2 μM) either in detergent solution (50 mM MOPS/K^+, pH 7.5, 20% glycerol, 0.02% DDM, 0.1 M NaCl) or embedded into nanodiscs in 50 mM MOPS, pH 7.5, was analyzed in the absence of co-factors and in the presence of ATP (10 mM) or ATP/$MgCl_2$ (10 mM/3 mM), LAO (11 μM) and L-arginine (1 mM). Samples were incubated for 20 min at 37 °C prior to spectroscopic analysis at 25 °C.

Five to seven measurements of each sample were recorded. The resulting decays were fitted with a three component model:

$$I(t) = \int_{-\infty}^{t} IRF\left(t'\right) \sum_{i=1}^{3} I_i e \frac{t-t'}{\tau_i} dt' \quad (3)$$

where I_i is the amplitude and τ_i is the lifetime of the i-th decay component. The lifetime components were fitted globally for each sample, resulting in τ_1 ~19 ns, τ_2 ~7 ns and τ_3 ~2 ns for detergent stabilized and τ_1 ~20 ns, τ_2 ~7 ns and τ_3 ~2 ns for reconstituted probes. Amplitude-weighted lifetimes for single curve fittings were calculated, averaged for each catalytical state and represented as mean ± standard deviation.

3. Results

3.1. Discrete conformations of HisQM(P-His_6)$_2$ can be visualized by limited proteolysis

In order to study conformational changes of the histidine transporter during the transport cycle, we used limited proteolysis with two different trypsin concentrations and incubation times, resulting in slow (Fig. 1A and B) and fast appearing degradation products (Fig. 1C and D). Three conditions of the transporter were monitored: the apo-state in plain buffer, the ATP-bound state, and the hydrolysis state which was obtained by the addition of MgATP and LAO/arginine.

In the long degradation assay (incubation with 3 μM trypsin for up to 8 min) the following observations were made (Fig. 1A and B): (i) $HisP_2$ is digested to a slightly smaller polypeptide, named P1, the occurrence of which is dependent on the state of the transport cycle. $HisP_2$ is most susceptible in the apo-state, while ATP-binding significantly slows down the rate of degradation. In the hydrolysis state only about one third of the digestion product is found compared to the ATP-bound state.

To exclude that degradation of HisP might at least in part be due to an excess of soluble HisP that is not associated with HisMQ, limited proteolysis was also performed with purified soluble $HisP_2$ under the same conditions as described above. Additionally, LAO/arginine was added to the ATP-bound state and also the MgADP-bound state was monitored. The digestion pattern shows (Fig. S1) that in the apo-state full length $HisP_2$ is almost completely degraded resulting in prominent peptide fragments < 20 kDa. Since these fragments are absent in the $HisQMP_2$ digestion pattern (Fig. 1A, lane 2), we conclude that the complex preparation contains if at all only negligible amounts of free $HisP_2$. The addition of nucleotide and Mg^{2+} ions has some stabilizing effect on $HisP_2$ as also observed with $HisQMP_2$ (Fig. 2A and B) suggesting that this effect occurs independently of HisQM but solely due to the closure of the HisP dimer thereby rendering the respective cleavage sites less susceptible. As expected, the addition of LAO had no effect on the digestion pattern confirming that binding of LAO is signaled through HisQM to the NBDs.

(ii) HisQ is degraded to fragment Q1 and subsequently Q2. Also this degradation is dependent on the state of the transporter, with Q1 being more stable in the hydrolysis state.

(iii) HisM is gradually degraded under all conditions tested up to 8 min of incubation with trypsin but a stable fragment could neither be detected by Coomassie staining nor by immunoblotting using an antiserum raised against the C-terminal peptide of HisM (F221-K235) (not shown).

In the short degradation assay (0.3 μM trypsin for up to 60 s) HisP and HisM appear to be stable (Fig. 1C and D). HisQ, on the other hand, is degraded to the slightly smaller fragment Q1, again very fast in the apo-state, more slowly in the ATP-bound form, and even more stabilized in the hydrolyzing complex. Fragment Q2 is not generated under these conditions.

To test if after trypsin degradation the subunits still form a complex despite the loss of part of HisQ, an aliquot was subjected to metal-affinity chromatography using a Talon resin (see Material and methods for details) directly after digestion. The result shows that mature HisP and HisM co-elute with fragment Q1 suggesting a stably assembled complex (Fig. S2).

It should be noted that LAO is completely stable under all conditions. LAO was given preference over HisJ because in contrast to the latter, it does not comigrate with fragment P1 in the SDS gel.

3.2. Conformational changes are also observed in a lipid environment

The above results indicated conformational changes of the transporter subunits especially under conditions of ATP hydrolysis, i.e. in the presence of LAO/arginine. However, in contrast to the transporter incorporated into proteoliposomes, LAO/arginine-stimulated ATPase activity is not observed in detergent solution [35] (Table 2). Thus, to investigate the effect of a lipid environment on the proteolytic cleavage pattern, we repeated key experiments with proteoliposomes containing $HisQMP_2$.

As shown in Fig. 2A, basically the same cleavage pattern and co-factor dependent protection against the protease under slow degradation conditions was observed as in detergent solution. The profile concerning HisP/P1 is less pronounced than in detergent solution probably because roughly only half of the transporter is oriented in the lipid bilayer with $HisP_2$ exposed to the medium and thereby accessible for the protease [36]. The observation that in the hydrolytic complex, binding of externally added LAO is protecting HisP despite the juxtaposing orientation can be explained by the presence of Mg^{2+} ions which make the vesicles leaky for ATP and substrate and even for small proteins [35]. An interesting feature is the stable accumulation of fragment Q2 compared to detergent solution (see Fig. 1A). This might be due to a putative cleavage site within Q2 which is not exposed to the protease in the lipid environment.

Due to the described inherent feature of proteoliposomes that transporter molecules are incorporated in two orientations and thus, only half of the potential tryptic cleavage sites are exposed to the medium, no clear pattern was obtained under fast degradation conditions. Consequently, we performed limited proteolysis with the transporter embedded in lipid nanodiscs [37]. Nanodiscs are composed of a phospholipid bilayer domain with two copies of an amphipathic membrane scaffold protein (MSP) that wrap around the periphery of the bilayer. They form by removal of detergent from initial detergent-phospholipid micelles. When a membrane protein is added it is trapped within the forming nanodisc structure. The advantage over proteoliposomes lies in the accessibility of the membrane protein from both sides of the bilayer.

Care has of course to be taken that the MSP itself is not cleaved by trypsin under the assay conditions. Kinetic analysis however revealed that the protein was fully stable up to 60 s (Fig. S3).

Fig. 2B illustrates that basically the same cleavage pattern and co-factor dependent protection against the protease is observed in nanodiscs as in detergent solution, albeit less pronounced. In the apo-state, some undigested HisQ is still detectable, which might be due to less flexible polypeptide chains in a lipid environment and thus reduced susceptibility to the protease. This notion is consistent with the results of a recent EPR analysis of the histidine transporter (Sippach, Weidlich, Klose, Schneider, Steinhoff, unpublished) and findings for members of other transporter families [38]. However, clear protection of HisQ against tryptic digestion as found in detergent solution (Fig. 1C and D) is also observed in

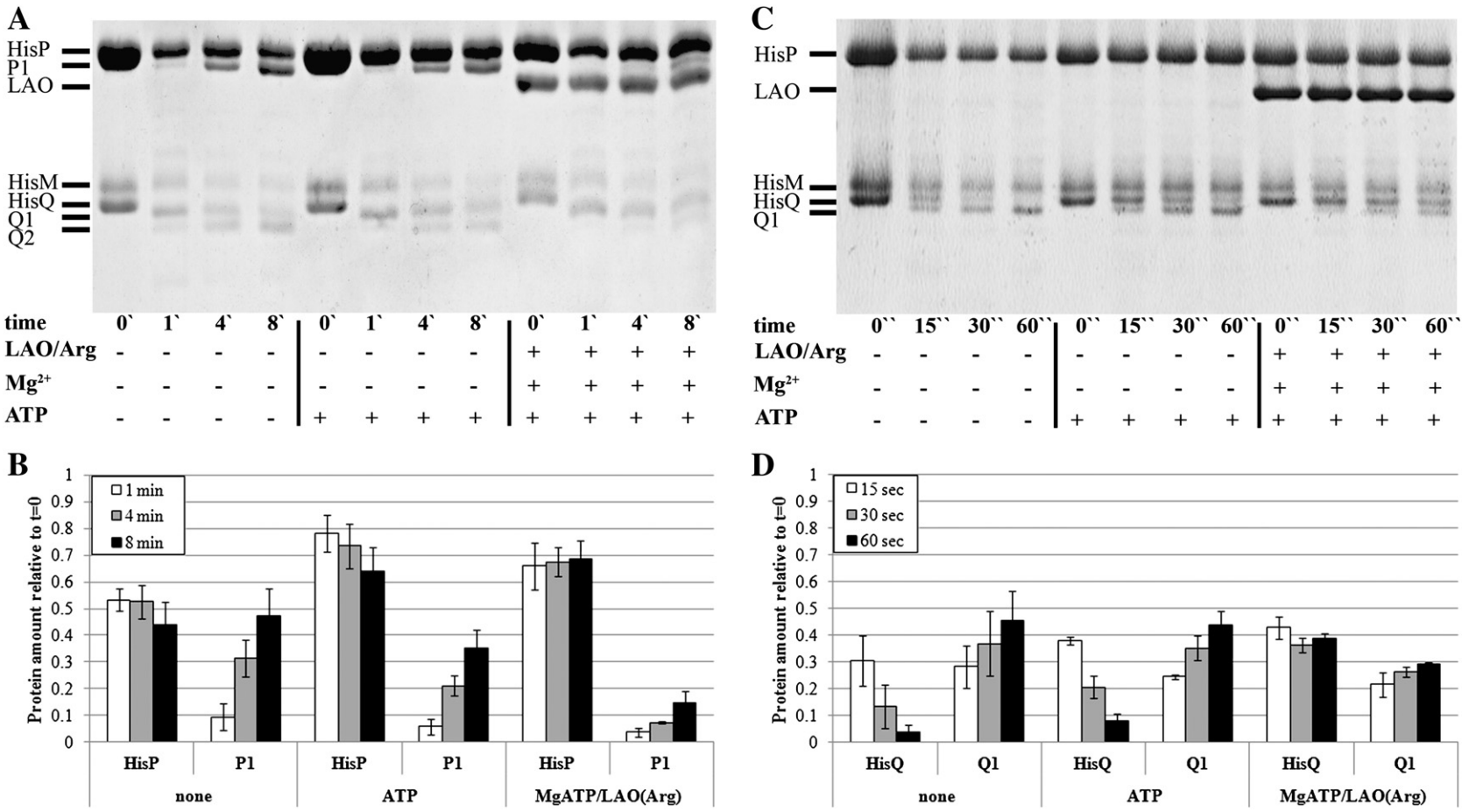

Fig. 1. Limited proteolysis of wild type $HisQMP_2$ in the absence and presence of co-factors. Wild type $HisQMP_2$ in detergent solution was incubated in the absence of co-factors, in the presence of ATP, and during hydrolysis. Trypsin was added to a final concentration of 3 μM (A) or 0.3 μM (C). Samples were taken at indicated times and subjected to SDS-PAGE. See 'Material and methods' for further details. Quantitation of mature proteins and cleavage products was carried out by pixel analysis of Coomassie-stained SDS gels from three independent experiments with Gelscan Standard V5.0 software. The units given are amounts of protein at the indicated time points relative to time point 0 of the degradation reaction. B. HisP/P1. D. HisQ/Q1.

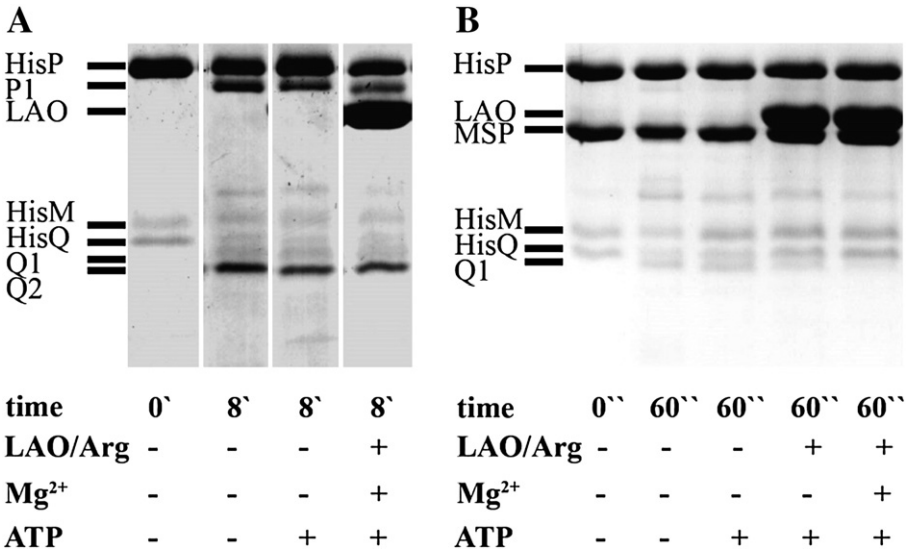

Fig. 2. Trypsin digestion pattern of $HisQMP_2$ in proteoliposomes and nanodiscs. $HisQMP_2$ was incorporated in proteoliposomes (A) or nanodiscs (B) to a concentration of 3 μM. LAO was added to the reaction mix to a concentration of 10 μM in the presence of 1 mM arginine. Limited proteolysis was essentially performed as described in the legend to Fig. 1. See 'Material and methods' for further details.

nanodiscs under pre-hydrolysis (LAO/arginine/ATP) and hydrolysis conditions. Faint protein bands appearing above HisM which probably derived from HisP were not further analyzed because no reproducible pattern could be obtained. Together, we conclude that digestion patterns observed in detergent solution are also detectable when the transporter is embedded in a lipid bilayer.

Table 2
ATPase activities of histidine transporter variants.

Variant protein	LAO/ arginine	ATPase activity (μmol P_i min^{-1} mg^{-1})	Stimulation by LAO/ arginine (n-fold)
Detergent solution			
$HisQMP_2$ wild type	−	0.097 ± 0.032	−
	+	0.096 ± 0.005	
$HisQMP(E179Q)_2$	−	0.0090 ± 0.0014	−
	+	0.0014 ± 0.0069	
$HisQMP(T205A)_2$	−	0.645 ± 0.124	−
	+	0.540 ± 0.073	
$HisQMP(K258H)_2$	−	0.057 ± 0.010	−
	+	0.084 ± 0.012	
$HisQ(R217H, R218H)MP_2$	−	0.054 ± 0.010	−
	+	0.051 ± 0.008	
$HisP_2$	−	0.025 ± 0.004	n.a.
Proteoliposomes			
$HisQMP_2$ wild type	−	0.119 ± 0.01	4.25
	+	0.698 ± 0.03	
$HisQMP(E179Q)_2$	−	0.025 ± 0.021	−
	+	0.005 ± 0.012	
$HisQMP(T205A)_2$	−	3.027 ± 0.158	−
	+	2.968 ± 0.182	
$HisQMP(K258H)_2$	−	0.380 ± 0.025	2.97
	+	1.129 ± 0.067	
$HisQ(R217H, R218H)MP_2$	−	0.320 ± 0.032	3.13
	+	1.003 ± 0.052	
$HisQ(R218C)M^*P^*_2$	−	0.040 ± 0.003	6.22
	+	0.249 ± 0.008	
$HisQ(R218C-32)M^*P^*_2$	−	0.115 ± 0.013	2.47
	+	0.284 ± 0.009	
Nanodiscs			
$HisQMP_2$ wild type	−	0.160 ± 0.041	3.2
	+	0.512 ± 0.091	
$HisQ(R218C-32)M^*P^*_2$	−	0.036 ± 0.001	4.03
	+	0.145 ± 0.007	

SE mean ($n \geq 3$). * denotes cys-less variant; n.a., not applicable.

3.3. Identification of proteolytic fragments and cleavage sites by mass spectrometry and mutational analysis

To identify the tryptic cleavage sites resulting in the observed proteolytic fragments of HisP and HisQ, stained protein bands were excised from gel slices and analyzed by mass spectrometry. Fragments P1, Q1 and Q2 were verified as derived from HisP and HisQ, respectively (Fig. 3A). While Q1 and P1 resulted from cutting off rather short peptides, Q2 seems to encompass the core helices 2, 3 and 4. Interestingly, once formed, this core region is very stable in a lipid environment and less stable in detergent solution, indicating that it is well buried in the lipid bilayer (Fig. 2A).

Trypsin cleaves proteins at the C-terminal end of arginine and lysine residues. Since mass spectrometry does not necessarily cover all peptides derived from trypsin digestion, peptides located N- or C-terminally might not be detected and thus, both ends of the fragments cannot be determined with accuracy as long as there are additional lysines or arginines present. Therefore, all the potential cleavage sites for P1 and Q1 were mutated to histidines in the *hisP* and *hisQ* genes, followed by purification of the respective transporter variants. Subsequently, trypsin digestion was performed under conditions, where the fragments were found to be most abundant (P1: 8 min/3 μM trypsin/apo-state; Q1: 60 s/0.3 μM trypsin/apo-state). The immunoblot (for HisP/P1) and SDS gels (for HisP/P1 and HisQ/Q1) for those mutants that displayed resistance to trypsin (Fig. 3B) demonstrate that HisP is cleaved at a low ratio C-terminally of arginine 248 and lysine 254 but cleavage is completely suppressed when lysine 258 is mutated (Fig. 3B, left panel). Thus, all three sites are apparently susceptible to trypsin but the most distal (C-terminal) lysine, immediately preceding the His tag, is the preferred cleavage site in HisP (Fig. 3C, left panel). In the case of HisQ, one or both arginines at positions 217/218 are the recognition sites for trypsin since cleavage is no longer observed after mutating these residues to histidines (Fig. 3B and C, right panel). (Please note that the mutations caused HisQ to migrate faster in the SDS gel.) Measuring ATPase activity of the complex variants in detergent solution and reconstituted in proteoliposomes assured that the mutations did not affect transporter function (not shown). The possible cleavage site(s) resulting in fragment Q2 were not further verified since compared to Q1 it was less indicative for defined states of the transport cycle.

Both confirmed main cleavage sites are located close to the respective C-terminal ends of the proteins as shown in a homology model of $HisQMP_2$ [39] which is based on the crystal structure of the *E. coli*

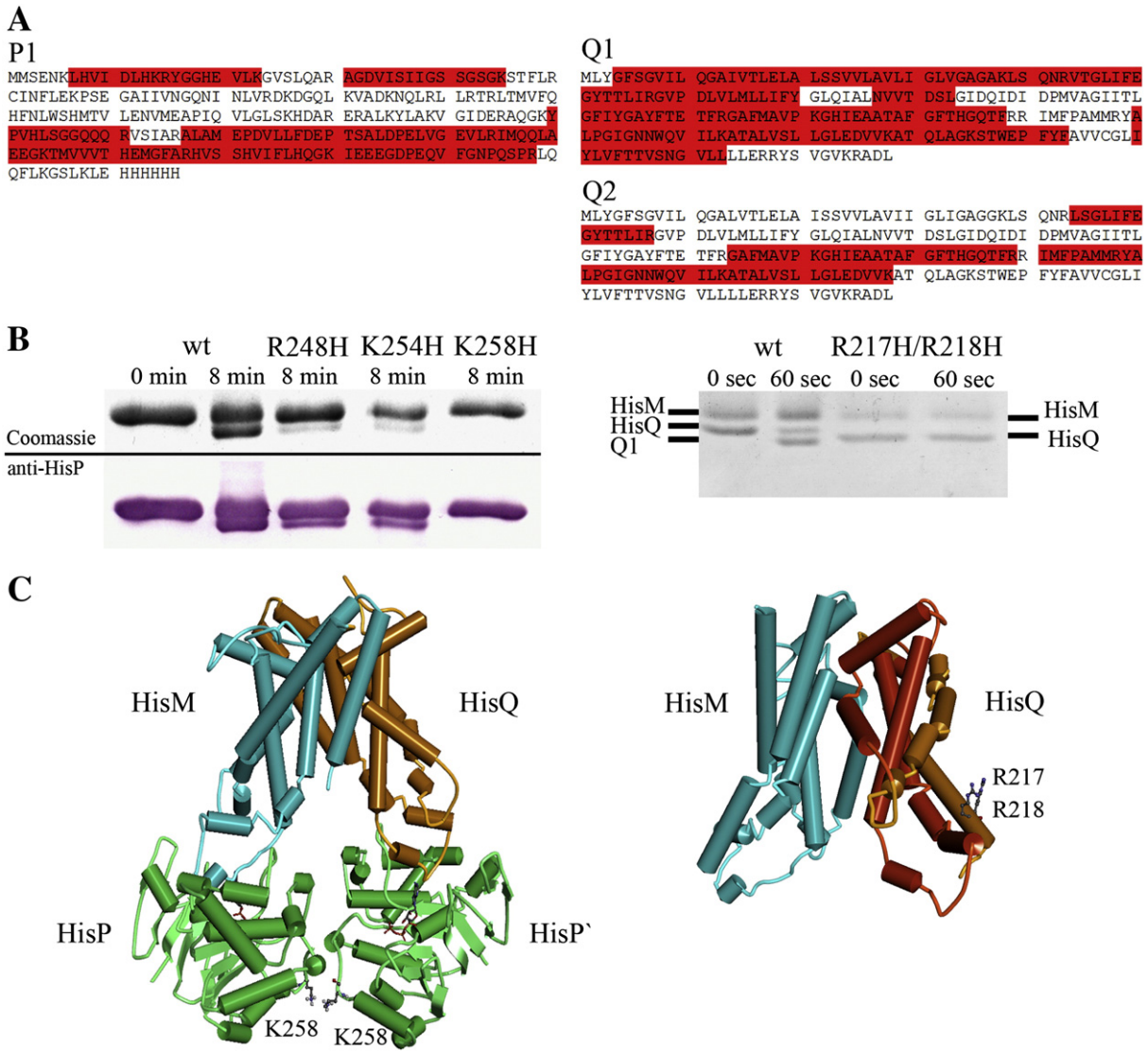

Fig. 3. Identification of the tryptic cleavage fragments and their cleavage sites by mass spectrometry and mutational analysis. A. Fragments P1, Q1, and Q2 were excised from the Coomassie-stained SDS gel and analyzed by mass spectrometry following total digestion with trypsin (P1, Q2) or chymotrypsin (Q1) digestion. Identified fragments are highlighted in red. B. Limited proteolysis of potential cleavage site mutants under slow (HisP, left panel) and fast (HisQ; right panel) degradation conditions analyzed by SDS-PAGE and immunoblotting (HisP only). C. Location of the confirmed cleavage sites (in ball-and-stick presentation) is shown in the homology model of $HisQMP_2$ (P-K258) and HisQM (Q-R217, Q-R218). $HisP_2$ is shown in green, HisM in blue and HisQ in brown. Fragment HisQ2 is indicated in red in the HisQM model (right panel).

methionine transporter MetNI (PDB ID: 3TUI) (Fig. 3C). In case of HisP, virtually the His-tag is removed by trypsin after the final helix which probably interacts with the opposing HisP monomer.

3.4. HisP and HisQ are most protected against trypsin during hydrolysis

Since the results described above proved the suitability of limited proteolysis to detect distinct conformations of the transporter, we investigated cofactor-dependent cleavage pattern in more detail. To this end, degradation of HisP was analyzed under long degradation conditions (3 μM trypsin/8 min) with the detergent solubilized complex while short degradation conditions (0.3 μM trypsin/60 s) to study the fate of HisQ were applied to the transporter both in detergent micelles and in nanodiscs. As shown in Fig. 4, the following conclusions can be drawn: HisP is most stabilized under hydrolytic and post-hydrolytic conditions, e.g. in the presence of LAO/arginine, Mg^{2+} ions and ATP or ADP (Fig. 4A and B, lanes 4 and 5). A similar protective effect is observed with ATP in the presence of LAO/arginine, representing the pre-hydrolysis state (Fig. 4A and B, lane 3). Under the latter conditions and in analogy to what was found for the maltose transporter [12,40–42], the HisP dimer is supposed to be fully closed while upon ATP hydrolysis the transporter is thought to reside in a semi-open state. Thus, the extreme C-terminus of HisP changes conformation during catalysis, being less exposed to the medium in the pre-, post- and hydrolytic state. Interestingly, already binding of arginine-loaded LAO caused some protection of HisP against trypsin (Fig. 4A and B, lane 7), thus communicating the availability of substrate across the membrane to the NBDs. This observation is consistent with results of a previous study using far-UV CD spectroscopy to demonstrate secondary structural changes of the histidine transporter in the presence of HisJ only [26].

Similar results were obtained for HisQ. While in the apo-state (no cofactors added), HisQ was completely converted to Q1 (Fig. 4C and D, lane 1), under hydrolytic and post-hydrolytic conditions, the amount of HisQ was 2-3fold higher than that of Q1 (Fig. 4C and D, lane 5). Consequently, residues Arg-217 and Arg-218 are protected against proteolytic attack, suggesting a motional change of helix 5 upon ATP hydrolysis. In the presence of LAO/arginine only (Fig. 4C and D, lane 7), the amount of Q1 was in between that of the apo- and hydrolytic states, similar to what was observed for P1. Thus, LAO is able to bind to the transporter in the apo-state, thereby provoking a change in

conformation of the NBDs at the cytoplasmic side and rendering the conformation of the TMDs half way from inward- to outward-facing. In the presence of LAO/arginine and ATP, representing the pre-hydrolytic state (Fig. 4C and D, lane 3), the cleavage pattern resembles that of the hydrolytic and post-hydrolytic state (lanes 4 and 5), although HisQ was overall more susceptible to trypsin.

In agreement with these results, the digestion of HisQ when analyzed in nanodiscs is most limited under pre-hydrolytic conditions (Fig. 4E and F, lane 4) and during hydrolysis (Fig. 4E and F, lane 5). Thus, motional changes of the TMDs as observed in detergent solution are basically reflecting those in a lipid environment.

Together, these results indicate that there are differentially susceptible cleavage sites in the NBDs and TMDs allowing the detection of a variety of conformers, presumably going along with open, semi-closed and closed states of the transporter during the cycle. Interestingly, similar experiments with the maltose transport complex showed a different pattern: the TMDs and MalFG were more protected in the apo-state than in the ATP-bound complex or post-hydrolytic state [43]. This is explainable by the location of the respective cleavage sites in the large periplasmic loops P1 and P2 of MalG and MalF, respectively, which are absent in HisQM. These loops are apparently more exposed to the solvent when the NBDs ($MalK_2$) reside in the closed (ATP-bound) conformation. In particular, this might coincide with the observation that MalF-P2 undergoes a conformational change upon concomitant binding of substrate-loaded binding protein and ATP [44].

3.5. Fluorescence lifetime spectroscopy confirms motional changes of HisQ

The proteolysis data revealed reduced susceptibility of the tryptic cleavage site of HisQ (R217/R218) (Fig. 3C, right panel) located at the cytoplasmic side of the membrane upon ATP binding and hydrolysis. This finding indicates a reorientation of transmembrane helix 5 during the translocation cycle. To obtain further proof for this notion, we performed fluorescence lifetime spectroscopy with a transporter variant containing a cysteine residue at position 218 of HisQ, thus allowing site-specific labeling with the fluorophore acyl-DBD-maleimide. DBD dyes are fluorescent probes which can be used to sense even small polarity changes since their fluorescence lifetime is highly influenced by the polarity of their microenvironment [33,34]. Fig. 5 presents the average amplitude weighted fluorescence lifetimes (τ_{AV}) of acyl-DBD labeled HisQ(R218C)MP_2 in detergent solution and after reconstitution in nanodiscs. The mean lifetimes for detergent stabilized transporters were 6.2 ns in the apo-state, 6.5 ns the in ATP-bound sate and 6.6 ns under hydrolyzing conditions. The mean lifetimes for nanodisc reconstituted transporters analyzed under the same conditions were 5.7, 6.1 and 6.3 ns, respectively. Hence, the fluorescence spectroscopy results are confirming discrete conformational states of the transporter as found by limited proteolysis. As indicated by an increase in fluorescence lifetime of the dye, HisQ(R218) is exposed to a less polar environment upon binding of ATP which is even more pronounced after ATP hydrolysis. Possibly, these changes may be explained by exclusion of water molecules from the local environment of the residue. Interestingly, the increase in fluorescent lifetime from apo- to ATP-bound state in nanodiscs is more than twice as high ($\Delta\tau = 0.3$–0.4 ns) as the lifetime increase from ATP-bound to hydrolysis state ($\Delta\tau = 0.1$–0.2 ns). This displays a larger change upon ATP binding in comparison to that of ATP hydrolysis and is also consistent with the findings from limited proteolysis (e.g. compare lanes 1, 2 and 4 in Fig. 4C). The higher absolute values of fluorescent lifetime in the case of detergent stabilized

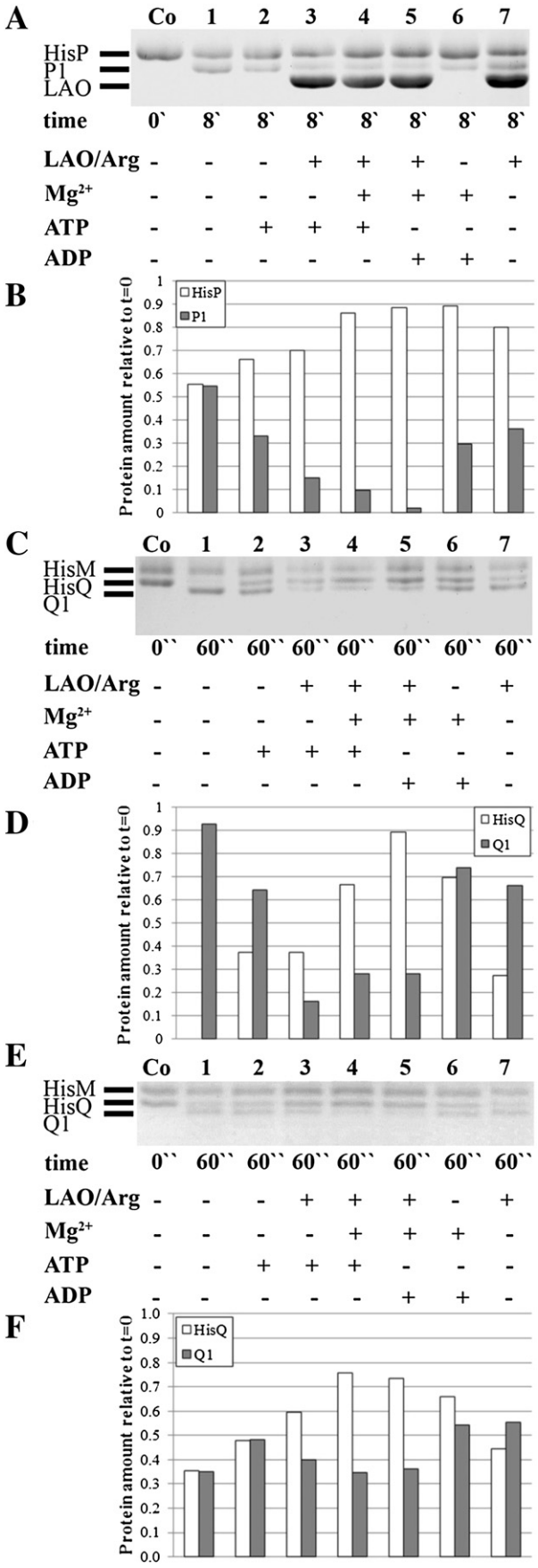

Fig. 4. Limited proteolysis of $HisQMP_2$ under various conditions. Limited proteolysis was performed with complex protein in detergent micelles (A, C) or embedded in nanodiscs (E) in the absence or presence of co-factors as indicated. Protein samples were taken at time points 0 (control), 8 min (HisP) (A) or 60 s (HisQ) (C, E), subjected to SDS-PAGE and the resulting fragments P1 (B) and Q1 (D, F) were subsequently quantified relative to the mature proteins by pixel analysis as described in the legend of Fig. 1. See 'Material and methods' for further details. Co, control. Representative gels are shown.

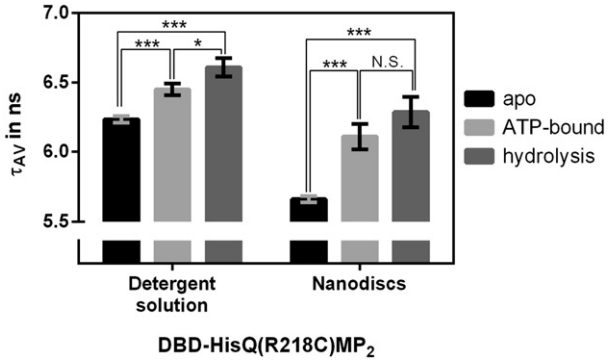

Fig. 5. Fluorescence lifetime spectroscopy of DBD-HisQ(R218C)MP_2. The amplitude weighted fluorescence lifetime averages of DBD-labeled HisQ(R218C)MP_2 with standard deviation (28 measurements in detergent solution, 10 measurements in nanodiscs) are shown in different states of the transport cycle. The average lifetime increases upon ATP binding and hydrolysis for both, detergent stabilized and nanodisc-reconstituted DBD-HisQ(R218C)MP_2. See 'Material and methods' for details. The data were analyzed using a Mann–Whitney U-test ($p < 0.001$ = ***, $p < 0.01$ = **, $p < 0.05$ = *).

compared to reconstituted transporters can be explained with different microenvironments after reconstitution. Nevertheless, the same environmental changes have been observed for the transporter both in detergent micelles and embedded in nanodiscs, thus strongly suggesting again that the properties of the histidine transporter in detergent solution reflect those in a lipid environment.

3.6. Proteolytic digestion patterns of complex variants display deviations from wild type

Having established limited proteolysis as a tool to detect distinct conformations of the histidine transporter during the transport cycle, we set out to apply the technique to transporter variants with different phenotypes: (i) The HisQMP(E179Q)$_2$ variant is mutated in the catalytic carboxylate whose function is to orient the water molecule which is attacking the γ-phosphate of ATP [24]. Therefore this mutant, like the analogous mutant (MalK-E159Q) of the maltose transport system [6,45], binds ATP while not being able to hydrolyze it. Moreover, in the crystal structure of the respective maltose transporter mutant, substrate was already released to its binding site in the MalF subunit and, consequently, the binding protein was found in its open conformation. Thus, it is assumed to represent a catalytic intermediate [6]; (ii) the HisQMP(T205A)$_2$ mutant was described earlier as binding protein-independent variant with high intrinsic ATPase activity that is coupled to transport [46,47], although further activation was observed in the presence of HisJ/histidine, suggesting that SBP can still interact with the complex. The mutants were purified and analyzed for their expected ATPase activities in detergent solution and in proteoliposomes, which confirmed the described phenotypes (Table 2). Fig. 6 shows the results of limited proteolysis performed with the variants under slow and fast degradation conditions.

The ATPase-deficient mutant HisQM(P-E179Q)$_2$ exhibited higher resistance of HisP and HisQ against trypsin compared to wild type under all conditions, but being most resistant in the absence of co-factors. This finding is consistent with the notion that the mutant's NBDs are locked in the closed conformation mimicking the ATP-bound state [6]. Our results demonstrate that this conformation also affects the relative exposure of helix 5 of HisQ. Furthermore, under conditions promoting hydrolysis, although ATP is not hydrolyzed by the mutant, stabilization of HisP and HisQ is more comparable to wild type indicating that binding of LAO is still signaled to the cytoplasmic side of the complex. The findings for E179Q match the results of limited proteolysis and crosslink studies with the maltose transporter [43,45] and are consistent with the crystal structure of MalE-FGK(E159Q)$_2$ [6].

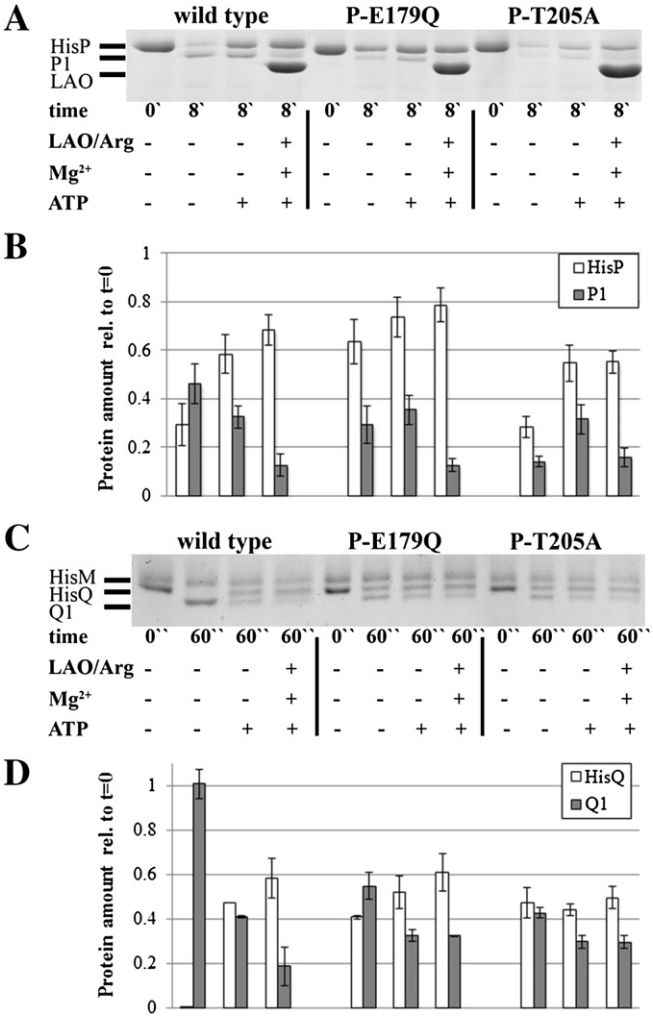

Fig. 6. Tryptic digestion profiles of histidine transporter variants. The indicated variants were subjected to limited proteolysis under slow (HisP) (A) and fast (HisQ) (C) degradation conditions in the absence and presence of co-factors as indicated. Quantitation of fragments following SDS-PAGE (B, D) was performed as described in the legend of Fig. 1.

In contrast, the binding protein-independent mutant HisQMP (T205A)$_2$ generally displayed higher susceptibility of HisP to trypsin, especially in the apo-state, suggesting a less stable overall structure. This finding is in line with the previous notion that the T205A mutation renders the transport complex more flexible [47] resulting e.g. in partial uncoupling from activating stimuli like binding of the SBP [48]. Interestingly, this phenotype is not seen with HisQ that exhibits normal overall stability but nevertheless also lacks a typical apo-state conformation, probably because the inward-facing conformation of the TMDs depends on the open conformation of the NBDs.

4. Discussion

We have demonstrated that limited proteolysis is a suitable tool to unravel conformational changes of HisQMP_2 in different states of the ATPase/transport cycle. One and two transiently stable cleavage fragments of HisP and HisQ, respectively, were observed, of which P1 and Q1 could be precisely identified. The cleavage sites have no functional relevance and are localized close to the carboxy-terminal ends of both subunits.

The C-terminal domain of HisP is short compared to the NBDs of e.g. the maltose or methionine transporters whose C-terminally extended peptide regions have additional regulatory functions [49,50]. In the

crystal structure of the molybdate transporter the similarly short C-terminal helices of the NBD dimers intertwine with each other and probably do not separate during ATP binding/hydrolysis but tilt around a hinge at the C-terminus [5]. Possibly, the C-terminal helices of HisP form a similar hook-like fold and such a twist makes the lysine 258 in HisP differentially susceptible to trypsin. In HisQ the last (5th) helix which probably extends into the cytoplasm is cleaved at one or both of the arginines which are surface exposed according to the structural model. Since the cleavage site is exposed in the apo-state but more concealed in the ATP-bound complex and in the hydrolytic complex, our results from limited proteolysis and fluorescence lifetime spectroscopy might indicate reorientation of helix 5 of HisQ and/or a closer packing of the complex protein upon NBD dimer closure. Results of a recent EPR study also point to a reorientation of helices within HisQM rather than a simple unidirectional opening–closing event of the two halves of the transporter (Sippach, Weidlich, Klose, Schneider, Steinhoff, unpublished data). Sequence alignment of helix 5 of HisQ with C-terminal peptides of not only closely related proteins but also including MetI and ModB, revealed, with two exceptions, conservation of at least one positively charged residue homologous to HisQ-R218 next to a glutamate or aspartate (Fig. S4). Moreover, in the C-terminal helix of MalG, an arginine residue (R283) is present which in the crystal structures of the maltose transporter in the apo- (PDB ID: 3FH6) and pre-hydrolysis state (PDB ID: 2R6G) is exposed to the medium. Although these data imply that, in contrast to HisQ, the carboxy-terminal helix of MalG does not change conformation upon binding of ATP and MalE/maltose, a tryptic fragment similar to Q1 was not obtained [43]. Rather, a cleavage site in periplasmic loop P1 was identified in MalG, indicating that the mobility of the helix in detergent solution differs from what is observed in the crystal structure. Interestingly, two arginine residues are also present at homologous positions of the HisM subunit. Since no cleavage products corresponding to Q1 and Q2 were obtained, our data suggest a different conformation of the C-terminal peptide of HisM compared to HisQ. Trypsin digestions with the closely related arginine transporter Art$(MP)_2$ suggest similar cleavage sites in the TMD ArtM and the NBD ArtP [39]. Here, ArtP is also more protected in pre-hydrolytic and hydrolytic state, indicating comparable motional changes. ArtM cleavage shows no differential pattern upon ATP/SBP-addition/hydrolysis what again points to different conformations/movements of the C-terminal helix of the TMDs of different transporters provided that the trypsin cleavage site is homologous to HisQ(R217/R218) [39]. The cleavage pattern of $HisQMP_2$ clearly allowed to distinguish the apo-state from the pre-, post-, and hydrolytic states while conformational changes triggered by ATP hydrolysis are apparently not accompanied by a change in exposure of the cleavage sites to the protease. Moreover, increased resistance of $HisP_2$ and HisQ to trypsin in the presence of liganded LAO reflects transmembrane signaling as observed for the maltose transport complex [43,44]. Moreover, the transporter variants exhibit differential proteolytic pattern explaining and confirming their deviant characteristics.

Together, despite the structural differences between the maltose and histidine transporters, our data suggest similar conformational changes during the transport cycle.

Acknowledgements

We thank Heidi Landmesser and Gabriele Brune (both from Humboldt Universität zu Berlin) for excellent technical assistance. This work was supported by the Deutsche Forschungsgemeinschaft (PAK 459, SCHN 274/14-1 to E.S. and PAK 459/2 - HE 3763/13-2 to A.H.).

Appendix A. Supplementary data

Supplementary data to this article can be found online at http://dx.doi.org/10.1016/j.bbamem.2013.08.024.

References

[1] In: E.B. Holland, S. Cole, K. Kuchler, C.F. Higgins (Eds.), ABC Proteins: From Bacteria to Man, Elsevier, Amsterdam, 2003.
[2] A.L. Davidson, E. Dassa, C. Orelle, J. Chen, Structure, function, and evolution of ATP binding cassette systems, Microbiol. Mol. Biol. Rev. 72 (2008) 317–364.
[3] T. Eitinger, D.A. Rodionov, M. Grote, E. Schneider, Canonical and ECF-type ATP binding cassette importers in prokaryotes: diversity in modular organization and cellular functions, FEMS Microbiol. Rev. 35 (2011) 3–67.
[4] K. Locher, Structure and mechanism of ATP-binding cassette transporters, Philos. Trans. R. Soc. Lond. B Biol. Sci. 364 (2009) 239–245.
[5] K. Hollenstein, D.C. Frei, K.P. Locher, Structure of an ABC transporter in complex with its binding protein, Nature 446 (2007) 213–216.
[6] M.L. Oldham, D. Khare, F.A. Quiocho, A.L. Davidson, J. Chen, Crystal structure of a catalytic intermediate of the maltose transporter, Nature 450 (2007) 515–522.
[7] D. Khare, M. Oldham, C. Orelle, A.L. Davidson, J. Chen, Alternating access in maltose transporter mediated by rigid-body rotations, Mol. Cell 33 (2009) 528–536.
[8] A. Licht, E. Schneider, ATP binding cassette systems: structures, mechanisms, and functions, Cent. Eur. J. Biol. 6 (2011) 785–801.
[9] O. Lewinson, A.T. Lee, K.P. Locher, D.C. Rees, A distinct mechanism for the ABC transporter BtuCD-BtuF revealed by the dynamics of complex formation, Nat. Struct. Mol. Biol. 17 (2010) 332–338.
[10] M.L. Daus, S. Berendt, S. Wuttge, E. Schneider, Maltose binding protein (MalE) interacts with periplasmic loops P2 and P1 respectively of the MalFG subunits of the maltose ATP binding cassette transporter (MalFGK(2)) from *Escherichia coli/Salmonella* during the transport cycle, Mol. Microbiol. 66 (2007) 1107–1122.
[11] M.L. Daus, M. Grote, E. Schneider, The MalF P2 loop of the ATP-binding cassette transporter $MalFGK_2$ from *Escherichia coli* and *Salmonella enterica* serovar Typhimurium interacts with maltose binding protein (MalE) throughout the catalytic cycle, J. Bacteriol. 191 (2009) 754–761.
[12] S. Böhm, A. Licht, S. Wuttge, E. Schneider, E. Bordignon, Conformational plasticity of the type I maltose ABC importer, Proc. Natl. Acad. Sci. U. S. A. 110 (2013) 5492–72013.
[13] B. Joseph, G. Jeschke, B.A. Goetz, K.P. Locher, E. Bordignon, Transmembrane gate movements in the type II ATP-binding cassette (ABC) importer BtuCD-F during nucleotide cycle, J. Biol. Chem. 286 (2011) 41008–41017.
[14] V.M. Korkhov, S.A. Mireku, K.P. Locher, Structure of AMP-PNP-bound vitamin B(12) transporter BtuCD-F, Nature 490 (2012) 367–372.
[15] E. Vigonsky, E. Ovcharenko, O. Lewinson, Two molybdate/tungstate ABC transporters that interact very differently with their substrate binding proteins, Proc. Natl. Acad. Sci. U. S. A. 110 (2013) 5440–5445.
[16] M.K. Doeven, G. van den Bogaart, V. Krasnikov, B. Poolman, Probing receptor-translocator interactions in the oligopeptide ABC transporter by fluorescence correlation spectroscopy, Biophys. J. 94 (2008) 3956–3965.
[17] G.F. Ames, Bacterial periplasmic transport systems: structure, mechanism, and evolution, Annu. Rev. Biochem. 55 (1986) 397–425.
[18] G.F.-L. Ames, K. Nikaido, I.X. Wang, P.-Q. Liu, C.E. Liu, C. Hu, Purification and characterization of the membrane-bound complex of an ABC transporter, the histidine permease, J. Bioenerg. Biomembr. 33 (2001) 79–92.
[19] E. Schneider, Import of solutes by ABC transporters-the maltose and other systems, in: ABC proteins: From bacteria to man, (E.B. Holland, S. Cole, K. Kuchler, C. Higgins, eds), 2003, pp. 157–185.
[20] E. Schneider, V. Eckey, D. Weidlich, N. Wiesemann, A. Vahedi-Faridi, P. Thaben, W. Saenger, Receptor-transporter interactions of canonical ATP-binding cassette import systems in prokaryotes, Eur. J. Cell Biol. 91 (2012) 311–317.
[21] R.E. Kerppola, G.F. Ames, Topology of the hydrophobic membrane-bound components of the histidine periplasmic permease. Comparison with other members of the family, J. Biol. Chem. 267 (1992) 2329–2336.
[22] B.H. Oh, C.H. Kang, H. de Bondt, S.H. Kim, K. Nikaido, A.K. Joshi, G.F. Ames, The bacterial periplasmic histidine-binding protein. Structure/function analysis of the ligand-binding site and comparison with related proteins, J. Biol. Chem. 269 (1994) 4135–4143.
[23] C.H. Kang, W.C. Shin, Y. Yamagata, S. Gokcen, G.F. Ames, S.H. Kim, Crystal structure of the lysine-, arginine-, ornithine-binding protein (LAO) from Salmonella typhimurium at 2.7-Å resolution, J. Biol. Chem. 266 (1991) 23893–23899.
[24] L.W. Hung, I.X. Wang, K. Nikaido, P.Q. Liu, G.F. Ames, S.H. Kim, Crystal structure of the ATP-binding subunit of an ABC transporter, Nature 396 (1998) 703–707.
[25] G.F. Ames, C.E. Liu, A.K. Joshi, K. Nikaido, Liganded and unliganded receptors interact with equal affinity with the membrane complex of periplasmic permeases, a subfamily of traffic ATPases, J. Biol. Chem. 271 (1996) 14264–14270.
[26] D.I. Kreimer, K.P. Chai, G.F. Ames, Nonequivalence of the nucleotide-binding subunits of an ABC transporter, the histidine permease, and conformational changes in the membrane complex, Biochemistry 39 (2000) 14183–14195.
[27] J.D. Campbell, S.S. Deol, F.M. Ashcroft, I.D. Kerr, M.S.P. Sansom, Nucleotide-dependent conformational changes in HisP: molecular dynamics simulations of an ABC transporter nucleotide-binding domain, Biophys. J. 87 (2004) 3703–3715.
[28] J.H. Miller, Experiments in Molecular Genetics, Cold Spring Harbor Laboratory Press, Cold Spring Harbor, NY, 1972.
[29] K.D. Tartoff, C.A. Hobbs, Improved media for growing plasmid and cosmid clones, Bethesda Res. Labs Focus 9 (1987) 12.
[30] V. Eckey, D. Weidlich, H. Landmesser, U. Bergmann, E. Schneider, The second extracellular loop of pore-forming subunits of ATP-binding cassette transporters for basic amino acids plays a crucial role in interaction with the cognate solute binding protein(s), J. Bacteriol. 192 (2010) 2150–2159.
[31] A. Vahedi-Faridi, V. Eckey, F. Scheffel, C. Alings, H. Landmesser, E. Schneider, W. Saenger, Crystal structures and mutational analysis of the arginine-, lysine-, histidine-binding protein ArtJ from *Geobacillus stearothermophilus*. Implications for

interactions of ArtJ with its cognate ATP-binding cassette transporter, Art $(MP)_2$, J. Mol. Biol. 375 (2008) 448–459.
[32] T.K. Ritchie, Y.V. Grinkova, T.H. Bayburt, I.G. Denisov, J.K. Zolnerciks, W.M. Atkins, S.G. Sligar, Reconstitution of membrane proteins in phospholipid bilayer nanodiscs, Methods Enzymol. 464 (2008) 211–232.
[33] P. Wessig, R. Wawrzinek, K. Möllnitz, E. Feldbusch, U. Schilde, A new class of fluorescent dyes based on 1,3-benzodioxole and [1,3]-dioxolo[4.5-f]benzodioxole, Tetrahedron Lett. 52 (2011) 6192–6195.
[34] R. Wawrzinek, P. Wessig, K. Möllnitz, J. Nikolaus, R. Schwarzer, P. Müller, A. Herrmann, DBD dyes as fluorescent probes for sensing lipophilic environments, Bioorg. Med. Chem. Lett. 22 (2012) 5367–5371.
[35] C.E. Liu, P.Q. Liu, G.F.-L. Ames, Characterization of the adenosine triphosphatase activity of the periplasmic histidine permease, a traffic ATPase (ABC transporter), J. Biol. Chem. 272 (1997) 21883–21891.
[36] C.E. Liu, G.F. Ames, Characterization of transport through the periplasmic histidine permease using proteoliposomes reconstituted by dialysis, Biol. Chem. 272 (1997) 859–866.
[37] T.H. Bayburt, S.G. Sligar, Membrane protein assembly into nanodiscs, FEBS Lett. 584 (2010) 1721–1727.
[38] I. Hänelt, D. Wunnicke, E. Bordignon, H.J. Steinhoff, D.J. Slotboom, Conformational heterogeneity of the aspartate transporter Glt(Ph), Nat. Struct. Mol. Biol. 20 (2013) 210–214.
[39] D. Weidlich, N. Wiesemann, J. Heuveling, K. Wardelmann, H. Landmesser, K. Behnam Sani, C. Worth, R. Preissner, E. Schneider, Residues of a proposed gate region in type I ATP-binding cassette import systems are crucial for function as revealed by mutational analysis, Biochim. Biophys. Acta 1828 (2013) 2164–2172.
[40] C. Orelle, T. Ayvaz, R.M. Everly, C.S. Klug, A.L. Davidson, Both maltose-binding protein and ATP are required for nucleotide-binding domain closure in the intact maltose ABC transporter, Proc. Natl. Acad. Sci. U. S. A. 105 (2008) 12837–12842.
[41] M.L. Oldham, J. Chen, Crystal structure of the maltose transporter in a pretranslocation intermediate state, Science 332 (2011) 1202–1205.
[42] G. Lu, J.M. Westbrooks, A.L. Davidson, J. Chen, ATP hydrolysis is required to reset the ATP-binding cassette dimer into the resting-state conformation, Proc. Natl. Acad. Sci. (USA) 102 (2005) 17969–17974.
[43] M.L. Daus, H. Landmesser, A. Schlosser, P. Müller, A. Herrmann, E. Schneider, ATP induces conformational changes of periplasmic loop regions of the maltose ATP-binding cassette transporter, J. Biol. Chem. 281 (2006) 3856–3865.
[44] M. Grote, Y. Polyhach, G. Jeschke, H.J. Steinhoff, E. Schneider, E. Bordignon, Transmembrane signaling in the maltose ABC transporter MalFGK2-E. Periplasmic MalF-P2 loop communicates substrate availability to the ATP-bound MalK dimer, J. Biol. Chem. 284 (2009) 17521–17526.
[45] M.L. Daus, M. Grote, P. Müller, M. Doebber, A. Herrmann, H.J. Steinhoff, E. Dassa, E. Schneider, ATP-driven MalK dimer closure and reopening and conformational changes of the "EAA" motifs are crucial for function of the maltose ATP-binding cassette transporter $(MalFGK_2)$, J. Biol. Chem. 282 (2007) 22387–22396.
[46] D.M. Speiser, G.F. Ames, *Salmonella typhimurium* histidine periplasmic permease mutations that allow transport in the absence of histidine-binding proteins, J. Bacteriol. 173 (1991) 1444–1451.
[47] P.Q. Liu, C.E. Liu, G.F. Ames, Modulation of ATPase activity by physical disengagement of the ATP-binding domains of an ABC transporter, the histidine permease, J. Biol. Chem. 274 (1999) 18310–18318.
[48] C.E. Liu, P.Q. Liu, A. Wolf, E. Lin, G.F.-L. Ames, Both lobes of the soluble receptor of the periplasmic histidine permease, an ABC transporter (traffic ATPase), interact with the membrane-bound complex, J. Biol. Chem. 274 (1999) 739–747.
[49] E. Bordignon, M. Grote, E. Schneider, The maltose ATP-binding cassette transporter in the 21st century — towards a structural dynamic perspective on its mode of action, Mol. Microbiol. 77 (2010) 1354–1366.
[50] N.S. Kadaba, J.T. Kaiser, E. Johnson, A. Lee, D.C. Rees, The high-affinity *E. coli* methionine ABC transporter: structure and allosteric regulation, Science 321 (2008) 250–253.